THE JOURNAL OF PHYSICAL CHEMISTRY Letters

Letter

pubs.acs.org/JPCL

Practical Model for First Hyperpolarizability Dispersion Accounting for Both Homogeneous and Inhomogeneous Broadening Effects

Jochen Campo,[†] Wim Wenseleers,*[,†] Joel M. Hales,[‡] Nikolay S. Makarov,[‡] and Joseph W. Perry[‡]

[†]Department of Physics, University of Antwerp (campus Drie Eiken), Universiteitsplein 1, B-2610 Wilrijk-Antwerpen, Belgium

[‡]School of Chemistry and Biochemistry and Center for Organic Photonics and Electronics (COPE), Georgia Institute of Technology, Atlanta, Georgia, United States

Supporting Information

ABSTRACT: A practical yet accurate dispersion model for the molecular first hyperpolarizability β is presented, incorporating both homogeneous and inhomogeneous line broadening because these affect the β dispersion differently, even if they are indistinguishable in linear absorption. Consequently, combining the absorption spectrum with one free shape-determining parameter G_{inhom}, the inhomogeneous line width, turns out to be necessary and sufficient to obtain a reliable description of the β dispersion, requiring no information on the homogeneous (including vibronic) and inhomogeneous line broadening mechanisms involved, providing an ideal model for practical use in extrapolating experimental nonlinear optical (NLO) data. The model is applied to the efficient NLO chromophore picolinium quinodimethane, yielding an excellent fit of the two-photon resonant wavelength-dependent data and a dependable static value $\beta_0 = 316 \times 10^{-30}$ esu. Furthermore, we show that including a second electronic excited state in the model does yield an improved description of the NLO data at shorter wavelengths but has only limited influence on β_0.

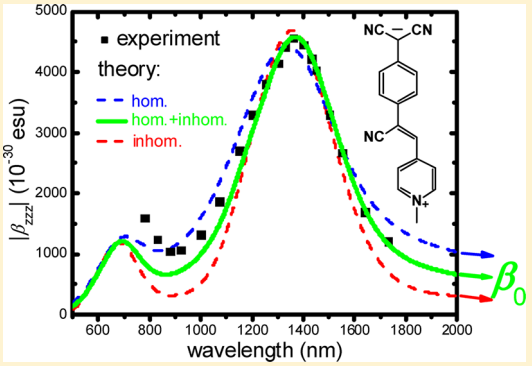

SECTION: Spectroscopy, Photochemistry, and Excited States

The search for second-order nonlinear optical (NLO) molecular materials focuses on noncentrosymmetric conjugated molecules, in which the highly mobile π-electrons give rise to a large NLO response (expressed by the molecular first hyperpolarizability β),[1,2] which is interesting for applications such as electro-optic modulators and switches and optical frequency convertors.[3−5] At the same time, such conjugated systems typically exhibit electronic transitions in the visible through the near-infrared (NIR) region, leading to pronounced resonances in the NLO response. As hyperpolarizability measurements (mainly by the technique of second-harmonic light scattering of randomly oriented molecules in liquid solution, or hyper-Rayleigh scattering, HRS)[6,7] are very often performed at a single wavelength in the NIR, the obtained β value is strongly influenced by (one- or two-photon) resonant enhancement. For a meaningful comparison of β between different molecules, and with theoretical values, it is important to correctly account for these resonance effects and extrapolate β to its static value β_0. While the simple two-level model (TLM)[8] is almost universally (yet inappropriately) used in the literature for this purpose, it is not applicable near resonance (where the most commonly used undamped TLM even diverges).[9,10] Therefore, there is a strong need for an appropriate theoretical β dispersion model, which can now be tested using detailed tunable wavelength HRS measurements that have recently become possible.[9−16] Previously, we performed such broad-band HRS measurements on the efficient zwitterionic NLO chromophore picolinium quinodimethane (PQDM) and fitted the results with simple models considering different line broadening mechanisms.[10] More complex β dispersion models do exist in the literature[17−19] and remain extremely useful when an in-depth understanding of the mechanisms involved is envisaged, but as they require a lot of additional parameters to be determined from extensive resonant Raman and hyper-Raman experiments, the two most physically realistic models developed in ref 10, namely, the purely homogeneous vibronic-like model and the single-mode vibronic model, are still the best available for practical use.[20−23] However, these two models include either maximum homogeneous or maximum inhomogeneous broadening, respectively, resulting in a too broad or too narrow β resonance and thus an over- or underestimation of the static hyperpolarizability β_0.[20] Hence, although these models represent a dramatic improvement over the TLM, quantitatively, the disparity is still too large to allow for reliable extrapolation.

In this work, our aim is to realize the ideal practical model that captures the essence of the physics determining the β dispersion and yields a quantitatively accurate description of it while keeping the number of free parameters to a minimum. To

Received: July 11, 2012
Accepted: July 31, 2012

   dx.doi.org/10.1021/jz300922r | J. Phys. Chem. Lett. 2012, 3, 2248−2252

do so, the key aspects of the above two models are generalized into a new, intermediate vibronic β model, where a single parameter allows for incorporation of the appropriate amount of homogeneous and inhomogeneous broadening to adjust the NLO resonance shape (without requiring a detailed description of the specific broadening mechanisms involved) while remaining strictly consistent with linear absorption. The resulting model is critically tested using the extensive wavelength-dependent HRS data for the zwitterionic PQDM chromophore.[10]

The two different vibronic models developed in our earlier work[10] for mapping out the molecular β dispersion are briefly resumed here to motivate and explain the development of the new intermediate vibronic model. All models presented here are based on the TLM[8] including homogeneous damping:[24,25]

$$\beta^{\mathrm{SHG}}(\omega, \omega_{\mathrm{eg}}, \gamma) = \beta_0 F(\omega, \omega_{\mathrm{eg}}, \gamma) \tag{1}$$

with

$$F(\omega, \omega_{\mathrm{eg}}, \gamma) = \frac{\omega_{\mathrm{eg}}^2}{3}\left[\frac{1}{(\omega_{\mathrm{eg}} + \mathrm{i}\gamma + 2\omega)(\omega_{\mathrm{eg}} + \mathrm{i}\gamma + \omega)} + \frac{1}{(\omega_{\mathrm{eg}} - \mathrm{i}\gamma - 2\omega)(\omega_{\mathrm{eg}} - \mathrm{i}\gamma - \omega)} + \frac{1}{(\omega_{\mathrm{eg}} + \mathrm{i}\gamma + \omega)(\omega_{\mathrm{eg}} - \mathrm{i}\gamma - \omega)}\right] \tag{2}$$

In this equation, ω_{eg} corresponds to the frequency of the (dominant) electronic transition, ω is the laser frequency, and γ is the homogeneous damping parameter (which is very small ($\sim$40 cm^{-1})[10] compared to the overall width of the absorption band). The static value β_0 is proportional to the dipole moment difference $\Delta\mu$ between the ground and excited states, which will be assumed to be equal for all vibrational sublevels.

In the purely homogeneous vibronic-like (HV) model,[10] the intramolecular charge-transfer (ICT) absorption band is described as a weighted sum of many narrow vibronic lines, so that β becomes an integral over all vibronic transitions contributing to the hyperpolarizability:[10]

$$\beta^{\mathrm{SHG}}(\omega, \gamma) \propto \Delta\mu \cdot \int \frac{\mathrm{Abs}(\omega'_{\mathrm{eg}})}{\omega'^{\,3}_{\mathrm{eg}}} F(\omega, \omega'_{\mathrm{eg}}, \gamma)\, \mathrm{d}\omega'_{\mathrm{eg}} \tag{3}$$

with ω'_{eg} running over the absorption band Abs(ω). In this model, no inhomogeneous effects are considered at all; therefore, the widths of the absorption band and β resonance peak originate entirely from the continuum of (very slightly homogeneously damped) vibronic levels. This typically results in an overestimation of the tails of the β resonance (see Figure 1).[10]

Another approach to include vibrational levels in a simple β dispersion model is to consider an electronic transition coupled linearly to just one normal mode and combine this with a maximal amount of inhomogeneous broadening G (giving a realistic description of the experimental absorption spectrum). In this inhomogeneous single-mode vibronic (IV) model,[10] absorption is described by a series of inhomogeneously broadened vibrational lines:[10]

$$\mathrm{Abs}(\omega) \propto \sum_n \omega_n \cdot W_n(S) \cdot \mathrm{e}^{-(\omega-\omega_n)^2/G^2} \tag{4}$$

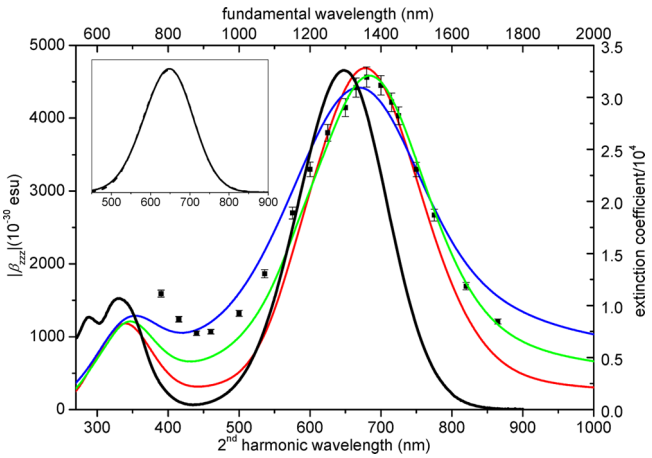

Figure 1. The purely homogeneous vibronic-like model (HV, blue),[10] the single-mode vibronic model (IV, red),[10] and the intermediate vibronic model (HIV, green) fitted to the experimental HRS data of PQDM (squares),[10] plotted together with the absorption spectrum (black line) at the second-harmonic wavelength. Only the experimental data at second-harmonic wavelengths $\geq$ 600 nm, that is, the two-photon resonant β values, were taken into account in the fitting procedure. In the HIV model, the absorption band is fitted by use of eq 4 with ω_{vib} fixed at 1550 cm^{-1} and G = 1435 cm^{-1}, λ_{00} (corresponding to ω_0) = 672 nm, and S = 0.65 as fit parameters. Both the overall amplitude and the deconvolution width G_{inhom} in eq 8 are optimized to fit the HRS data, yielding G_{inhom} = 1385 cm^{-1}. The inset shows the absorption band calculated using identical parameters as those for the HIV β model (dashed line), compared to the experimental spectrum (solid line), essentially coinciding.

where $W_n(S)$ is the relative intensity of the transition to the nth vibrational level of the excited state at $\hbar\omega_n = E_{\mathrm{eg}} + n\hbar\omega_{\mathrm{vib}}$, which can be modeled in terms of the vibronic coupling strength S as[26]

$$W_n(S) = \frac{S^n \mathrm{e}^{-S}}{n!} \tag{5}$$

The hyperpolarizability can then be written as a (inhomogeneous) convolution of a coherent sum of weakly homogeneously damped β contributions:[10]

$$(\beta^{\mathrm{SHG}}_{\mathrm{incoh}}(\omega))^2 = \int \frac{\mathrm{e}^{-x^2/G^2}}{G\sqrt{\pi}} \left|\left| \sum_n \beta_0^n \cdot F(\omega, \omega_n + x, \gamma) \right|\right|^2 \mathrm{d}x \propto \int \mathrm{e}^{-x^2/G^2} \left|\left| \sum_n \frac{\omega_n \cdot W_n(S)}{(\omega_n + x)^3} \cdot F(\omega, \omega_n + x, \gamma) \right|\right|^2 \mathrm{d}x \tag{6}$$

In contrast to the above HV model, this IV model incorporates maximum inhomogeneous broadening (for a vibronic model consistent with the given overall width of the linear absorption spectrum) and is found to yield a β resonance peak that is too narrow compared to the experiment (see Figure 1).[10] Due to the marked difference in widths, the best fits of the two extreme limiting models HV and IV shown in Figure 1 lead to very different static values β_0 (514 and 144 $\times$ 10^{-30} esu respectively), although this range is narrowed down when based on the least resonant data point (247–397 $\times$ 10^{-30} esu).[10] These observations strongly indicate that a new model combining the key features of the HV and IV models will yield an accurate description of the β dispersion, and in contrast to the more detailed models in the literature,[17−19] this will be

dx.doi.org/10.1021/jz300922r | J. Phys. Chem. Lett. 2012, 3, 2248−2252

realized here without the addition of a large number of parameters.

To construct such a vibronic β dispersion model including both homogeneous and inhomogeneous broadening (henceforth denoted as the HIV model), an amount of inhomogeneous broadening needs to be incorporated into the HV model. Obviously, this additional broadening cannot simply be added as this would result in too broad of an absorption band (and an even broader dispersion curve). In order to maintain consistency with the experimentally observed absorption spectrum Abs(ω), this spectrum is first deconvoluted with a Gaussian curve having a width G_{inhom} to obtain the hypothetical purely homogeneous absorption spectrum $\mathrm{Abs}_{\mathrm{hom}}(\omega)$ that would occur if no inhomogeneous broadening were present. A direct deconvolution of the experimental absorption spectrum is numerically treacherous, but a Gaussian deconvolution can be readily obtained from a multi-Gaussian fit of the absorption band (such as the vibronic series used above for the IV model, but as discussed below, also other multi-Gaussian fits can be used). The deconvoluted bands are also Gaussian but with narrower widths of $(G^2 - G_{\mathrm{inhom}}^2)^{1/2}$, leading to the following expression for the deconvoluted absorption band:

$$\mathrm{Abs}_{\mathrm{hom}}(\omega) \propto \sum_n \omega_n \cdot W_n(S) \cdot \mathrm{e}^{-(\omega-\omega_n)^2/G^2 - G_{\mathrm{inhom}}^2} \tag{7}$$

Using this $\mathrm{Abs}_{\mathrm{hom}}$ in combination with the Gaussian inhomogeneous broadening with width G_{inhom} is then, by definition, consistent with the experimental absorption spectrum. Hence, $\mathrm{Abs}_{\mathrm{hom}}$ can be inserted in the HV model (eq 3), and this entire expression can then be convoluted with the inhomogeneous distribution with width G_{inhom} (as in the IV model, eq 6), leading to the following expression for the HIV model:

$$(\beta_{\mathrm{incoh}}^{\mathrm{SHG}}(\omega, G_{\mathrm{inhom}}))^2 \propto \int \left| \int \frac{\mathrm{Abs}_{\mathrm{hom}}(\omega'_{\mathrm{eg}} + \Delta\omega)}{\omega'^{\,3}_{\mathrm{eg}}} F(\omega, \omega'_{\mathrm{eg}}, \gamma)\, \mathrm{d}\omega'_{\mathrm{eg}} \right|^2 \mathrm{e}^{-\Delta\omega^2/G_{\mathrm{inhom}}^2}\, \mathrm{d}\Delta\omega \tag{8}$$

Hence, apart from the overall amplitude, there is only a single free parameter G_{inhom} (inhomogeneous width), which allows for modifying the shape (i.e., the width) of the resonances. In the limit of small G_{inhom}, the HV model is reproduced, whereas the IV model curve is obtained if G_{inhom} approaches G (i.e., the Gaussian width of the individual vibrational bands).

With eq 8, a very good description of the low-energy resonance of PQDM is obtained (see Figure 1). The red shift between the two-photon resonance with the ICT band and the linear absorption maximum is in perfect agreement with the experiment, and also, the long wavelength tail is modeled very accurately, yielding a dependable static value β_0 of 316×10^{-30} esu (see Table S1 in the Supporting Information for a comparison between the different models), within the range of upper and lower bounds ($247-397 \times 10^{-30}$ esu; see above) set earlier by the two extreme limiting models.[10]

The multi-Gaussian fit of the absorption spectrum used above should not necessarily represent a physically realistic vibronic series but rather can be seen as a purely mathematical approach to facilitate the deconvolution. In general, this procedure is expected to give a reliable description of the β dispersion as long as a good multi-Gaussian fit of the experimental absorption spectrum is used and G_{inhom} is significantly smaller than each of the involved Gaussian widths G_i. Indeed, we also tried various other fits deliberately composed of significantly different individual Gaussian components (hence, different fit parameters) and found that the HIV model and its extrapolation to the static limit are not sensitive to the specific multi-Gaussian fit used (reproducing the same β_0 within 2%; see the Supporting Information). This insensitivity can be further explained by the fact that, even though slight differences in the fits of the absorption spectrum are amplified upon deconvolution, these differences are again averaged out by convolution in the actual β dispersion model.

To further test the reliability of this model, the influence of incorporating the higher-energy (HE) electronic transition observed in the absorption spectrum of PQDM at 330 nm (see Figure 1) was also explored (see Figure 2 and the Supporting Information), also using transient absorption spectroscopy to estimate the excited-state transition dipole moment involved. While this obviously improves the description of the short-wavelength HRS data, where the NLO response is increased by virtue of the doubly resonant contribution from this transition, the extrapolation to the static limit is not influenced much (~12% in the most plausible case of a near doubly resonant contribution or ~22% in the worst case of a second ICT state with a large two-level type contribution; see the Supporting Information).

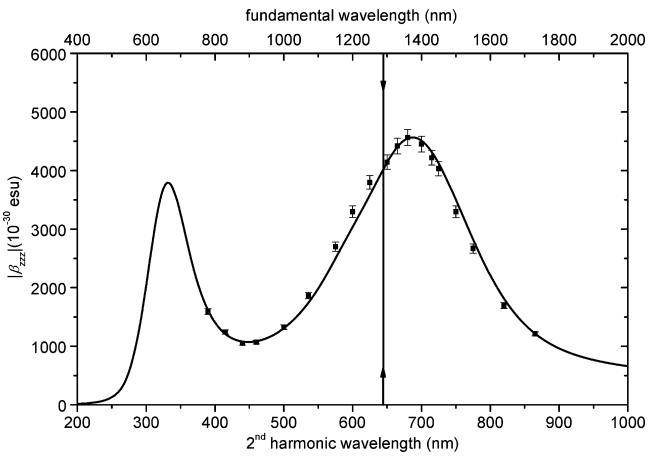

Figure 2. The HIV model extended with the inclusion of the higher-energy transition by means of a single homogeneously broadened three-level type term (curve; see the Supporting Information for details), fitted to the experimental HRS data of PQDM (squares). The vertical arrows indicate λ_{max} of the experimental ICT band.

In conclusion, a practically implementable dispersion model for the molecular first hyperpolarizability β is proposed, in which the shape of the β dispersion curve is determined solely by the linear absorption spectrum, and a single free parameter G_{inhom}, representing the amount of inhomogeneous broadening in the spectrum. This parameter is found to be necessary and sufficient to obtain an accurate description of the β dispersion as it captures the essence of the physics governing this dispersion, namely, the fact that different combinations of homogeneous and inhomogeneous broadening can lead to the same linear absorption spectrum yet have different effects on the shape of the β dispersion because they respectively lead to either a coherent (homogeneous) or incoherent (inhomogeneous) addition of contributions to the NLO response. Unlike more detailed models developed previously,[17−19] this model (HIV) does not require any knowledge of the actual

homogeneous (including vibronic) or inhomogeneous broadening mechanisms involved, which would introduce too many parameters for wide practical use. Rather, we propose to use the HIV model for extrapolation purposes, based on HRS measurements at at least two wavelengths, preferably one at and one as far as possible from resonance. If only a single wavelength measurement is available, the limiting cases with $G_{inhom} = 0$ (≡HV model[10]) and with maximal G_{inhom} (≡IV model[10]) can be used to estimate upper and lower limits to β_0, respectively, but when based on a measurement too close to resonance, the difference between these limiting cases can be on the order of a factor of 4 (note that the almost universally used undamped TLM[8] yields even much larger discrepancies between the static values based on experimental values at different wavelengths; see Table S1, Supporting Information). The reliability of the HIV model is demonstrated for PQDM, yielding a dependable static value β_0 of 316×10^{-30} esu, which (at least for this prototypical dipolar NLO chromophore) is moreover found to be insensitive to the extension of the model with a higher-energy transition, although the latter of course improves the description of the β dispersion at very short wavelengths. As such, the HIV model comprises an ideal combination of robustness, accuracy, and simplicity for general application in the routine analysis of experimental NLO data.

EXPERIMENTAL SECTION

The extensive wavelength-dependent HRS results for PQDM in *N*,*N*-dimethylformamide (DMF) solution are adopted from our earlier work,[10] where the experimental details can be found.

The femtosecond excited-state absorption spectrum for PQDM in DMF was acquired by means of a transient absorption spectroscopy system (Ultrafast Systems, Helios) coupled to an amplified laser system, similar to that described in detail before.[27,28] More experimental details can be found in the Supporting Information.

ASSOCIATED CONTENT

Supporting Information

Insensitivity of the HIV model to the fitting procedure of the linear ICT band. Comparison of the present models with previous practical models and with the almost universally used TLM. Influence of the incorporation of the higher-energy transition in the HIV model. Transient absorption spectroscopy for PQDM. This material is available free of charge via the Internet at http://pubs.acs.org.

AUTHOR INFORMATION

Corresponding Author

*E-mail: Wim.Wenseleers@ua.ac.be.

Notes

The authors declare no competing financial interest.

ACKNOWLEDGMENTS

J.C. is a Postdoctoral Fellow of the Fund for Scientific Research of Flanders (FWO − Vlaanderen, Belgium) and performed a 1 year research stay at Georgia Tech in the framework of the Mobility Allowance of the FWO. Financial support from the Group Projects G.0129.07 and G.0206.12 and from the Research Grant of the FWO (#1526511N) is gratefully acknowledged.

REFERENCES

(1) Prasad, P. N.; Williams, D. J. *Introduction to Nonlinear Optical Effects in Molecules and Polymers*; John Wiley & Sons: New York, 1991.
(2) Zyss, J. *Molecular Nonlinear Optics: Materials, Physics, and Devices*; Academic Press: San Diego, CA, 1994.
(3) Shi, Y. Q.; Lin, W. P.; Olson, D. J.; Bechtel, J. H.; Zhang, H.; Steier, W. H.; Zhang, C.; Dalton, L. R. Electro-Optic Polymer Modulators with 0.8 V Half-Wave Voltage. *Appl. Phys. Lett.* **2000**, *77*, 1−3.
(4) Dalton, L. R.; Harper, A.; Ren, A.; Wang, F.; Todorova, G.; Chen, J.; Zhang, C.; Lee, M. Polymeric Electro-Optic Modulators: From Chromophore Design to Integration with Semiconductor Very Large Scale Integration Electronics and Silica Fiber Optics. *Ind. Eng. Chem. Res.* **1999**, *38*, 8−33.
(5) Chang, C. C.; Chen, C. P.; Chou, C. C.; Kuo, W. J.; Jeng, R. J. Polymers for Electro-Optical Modulation. *J. Macromol. Sci., Polym. Rev.* **2005**, *C45*, 125−170.
(6) Terhune, R. W.; Maker, P. D.; Savage, C. M. Measurements of Nonlinear Light Scattering. *Phys. Rev. Lett.* **1965**, *14*, 681−684.
(7) Clays, K.; Persoons, A. Hyper-Rayleigh Scattering in Solution. *Phys. Rev. Lett.* **1991**, *66*, 2980−2983.
(8) Oudar, J. L.; Chemla, D. S. Hyperpolarizabilities of Nitroanilines and Their Relations to Excited-State Dipole-Moment. *J. Chem. Phys.* **1977**, *66*, 2664−2668.
(9) Robalo, M. P.; Teixeira, A. P. S.; Garcia, M. H.; da Piedade, M. F. M.; Duarte, M. T.; Dias, A. R.; Campo, J.; Wenseleers, W.; Goovaerts, E. Synthesis, Characterisation and Molecular Hyperpolarisabilities of Pseudo-Octahedral Hydrido(Nitrile)Iron(II) Complexes for Nonlinear Optics: X-Ray Structure of $[Fe(H)(dppe)_2(4\text{-}NCC_6H_4NO_2)][PF_6]\cdot CH_2Cl_2$. *Eur. J. Inorg. Chem.* **2006**, 2175−2185.
(10) Campo, J.; Wenseleers, W.; Goovaerts, E.; Szablewski, M.; Cross, G. Accurate Determination and Modeling of the Dispersion of the First Hyperpolarizability of an Efficient Zwitterionic Nonlinear Optical Chromophore by Tunable Wavelength Hyper-Rayleigh Scattering. *J. Phys. Chem. C* **2008**, *112*, 287−296.
(11) Hung, S. T.; Wang, C. H.; Kelley, A. M. Resonant Raman Spectra and First Molecular Hyperpolarizabilities of Strongly Charge-Transfer Molecules. *J. Chem. Phys.* **2005**, 123.
(12) Shoute, L. C. T.; Helburn, R.; Kelley, A. M. Solvent Effects on the Resonance Raman and Hyper-Raman Spectra and First Hyperpolarizability of *N*,*N*-Dipropyl-*p*-nitroaniline. *J. Phys. Chem. A* **2007**, *111*, 1251−1258.
(13) Leng, W.; Kelley, A. M. Hyper-Rayleigh and Hyper-Raman Scatterings with Intermediate and Two-Photon Resonances. *J. Chem. Phys.* **2007**, 127.
(14) Campo, J.; Desmet, F.; Wenseleers, W.; Goovaerts, E. Highly Sensitive Setup for Tunable Wavelength Hyper-Rayleigh Scattering with Parallel Detection and Calibration Data for Various Solvents. *Optics Express* **2009**, *17*, 4587−4604.
(15) Zhu, J.; Lu, C. G.; Cui, Y. P.; Zhang, C. Z.; Lu, G. Y. Two-Photon Resonant Hyperpolarizability of an H-Shaped Molecule Studied by Wavelength-Tunable Hyper-Rayleigh Scattering. *J. Chem. Phys.* **2010**, 133.
(16) Campo, J.; Painelli, A.; Terenziani, F.; Van Regemorter, T.; Beljonne, D.; Goovaerts, E.; Wenseleers, W. First Hyperpolarizability Dispersion of the Octupolar Molecule Crystal Violet: Multiple Resonances and Vibrational and Solvation Effects. *J. Am. Chem. Soc.* **2010**, *132*, 16467−16478.
(17) Moran, A. M.; Egolf, D. S.; Blanchard-Desce, M.; Kelley, A. M. Vibronic Effects on Solvent Dependent Linear and Nonlinear Optical Properties of Push−Pull Chromophores: Julolidinemalononitrile. *J. Chem. Phys.* **2002**, *116*, 2542−2555.
(18) Shoute, L. C. T.; Bartholomew, G. P.; Bazan, G. C.; Kelley, A. M. Resonance Hyper-Raman Excitation Profiles of a Donor−Acceptor Substituted Distyrylbenzene: One-Photon and Two-Photon States. *J. Chem. Phys.* **2005**, 122.
(19) Shoute, L. C. T.; Blanchard-Desce, M.; Kelley, A. M. Resonance Hyper-Raman Excitation Profiles and Two-Photon States of a Donor−

Acceptor Substituted Polyene. *J. Phys. Chem. A* **2005**, *109*, 10503−10511.
(20) Xiong, Y.; Tang, H. D.; Zhang, J. D.; Wang, Z. Y.; Campo, J.; Wenseleers, W.; Goovaerts, E. Functionalized Picolinium Quinodimethane Chromophores for Electro-Optics: Synthesis, Aggregation Behavior, and Nonlinear Optical Properties. *Chem. Mater.* **2008**, *20*, 7465−7473.
(21) Mancois, F.; Pozzo, J. L.; Pan, J. F.; Adamietz, F.; Rodriguez, V.; Ducasse, L.; Castet, F.; Plaquet, A.; Champagne, B. Two-Way Molecular Switches with Large Nonlinear Optical Contrast. *Chem.—Eur. J.* **2009**, *15*, 2560−2571.
(22) de Meulenaere, E.; Asselberghs, I.; de Wergifosse, M.; Botek, E.; Spaepen, S.; Champagne, B.; Vanderleyden, J.; Clays, K. Second-Order Nonlinear Optical Properties of Fluorescent Proteins for Second-Harmonic Imaging. *J. Mater. Chem.* **2009**, *19*, 7514−7519.
(23) Sergeyev, S.; Didier, D.; Boitsov, V.; Teshome, A.; Asselberghs, I.; Clays, K.; Velde, C.; Plaquet, A.; Champagne, B. Symmetrical and Nonsymmetrical Chromophores with Troger's Base Skeleton: Chiroptical, Linear, and Quadratic Nonlinear Optical Properties—A Joint Theoretical and Experimental Study. *Chem.—Eur. J.* **2010**, *16*, 8181−8190.
(24) Orr, B. J.; Ward, J. F. Perturbation Theory of the Non-Linear Optical Polarization of an Isolated System. *Mol. Phys.* **1971**, *20*, 513−526.
(25) Berkovic, G.; Meshulam, G.; Kotler, Z. Measurement and Analysis of Molecular Hyperpolarizability in the Two-Photon Resonance Regime. *J. Chem. Phys.* **2000**, *112*, 3997−4003.
(26) Fowler, W. B. *Physics of Color Centers*; Academic Press Inc.: New York, 1968.
(27) Hales, J. M.; Cozzuol, M.; Screen, T. E. O.; Anderson, H. L.; Perry, J. W. Metalloporphyrin Polymer with Temporally Agile, Broadband Nonlinear Absorption for Optical Limiting in the Near Infrared. *Optics Express* **2009**, *17*, 18478−18488.
(28) Malicki, M.; Hales, J. M.; Rumi, M.; Barlow, S.; McClary, L.; Marder, S. R.; Perry, J. W. Excited-State Dynamics and Dye−Dye Interactions in Dye-Coated Gold Nanoparticles with Varying Alkyl Spacer Lengths. *Phys. Chem. Chem. Phys.* **2010**, *12*, 6267−6277.

Supporting Information for

A Practical Model for First Hyperpolarizability Dispersion Accounting for both Homogeneous and Inhomogeneous Broadening Effects

Jochen Campo,[†] *Wim Wenseleers,*[†,*] *Joel M. Hales,*[#] *Nikolay S. Makarov*[#] *and Joseph W. Perry*[#]

[†]Department of Physics, University of Antwerp (campus Drie Eiken), Universiteitsplein 1, B-2610 Wilrijk-Antwerpen, Belgium.

[#]School of Chemistry and Biochemistry and Center for Organic Photonics and Electronics (COPE), Georgia Institute of Technology, Atlanta, Georgia.

Wim.Wenseleers@ua.ac.be

1. Insensitivity of the HIV β model to the fitting procedure of the linear ICT band

To test the effect the choice of the absorption band fitting procedure has on the HIV model, several expressions other than the vibrational series (Eq. (4)) were used to fit this band, such as a series of Gaussians with increasing width, (i) with the same equidistant frequency-spacing as for the vibrational series (1550 cm^{-1}), and (ii) with an equidistant spacing of 1300 cm^{-1} (see Figure S1 and Table S1). In order to thoroughly test the robustness of the β model, the latter is taken deliberately beyond the physically realistic range: in general for a conjugated chain an effective frequency around 1400 cm^{-1} is expected, average between 1200 and 1600 cm^{-1} for single and double CC bonds, and in the present case of PQDM, a larger effective frequency is expected due to the contribution of the C≡N vibrations. In

each case a very good fit to the two-photon resonant HRS data is indeed obtained following implementation of the HIV model, also resulting in very comparable static values β_0 (see Table S1).

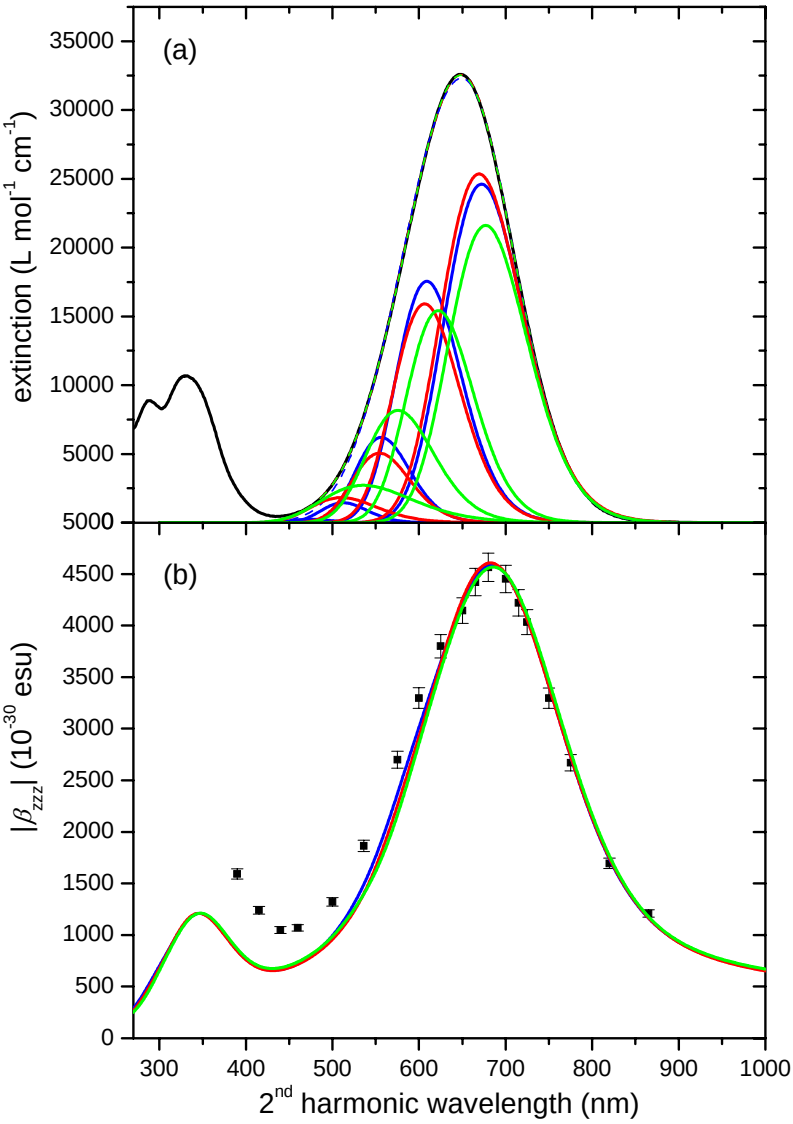

Figure S1. (a) Several Gaussian series fitted to the experimental ICT band of PQDM (black): the vibrational expression (Eq. (4), blue), and an equidistant series of Gaussians with increasing width, (i) with a frequency spacing of 1550 cm^{-1} (red), and (ii) with a spacing of 1300 cm^{-1} (green). The individual Gaussian components (solid curves; Gaussian functions of frequency) as well as their total sum (dashed curves, essentially coinciding) are shown. In each case, an additional Gaussian (not shown, and not used for the β models in (b)) was included to fit the absorption band at higher energy. **(b)** The corresponding HIV models (curves, essentially coinciding), fitted to the experimental HRS data of PQDM (squares) by optimizing both the overall amplitude and the deconvolution width G_{inhom}.

Table S1. Comparison of the present models (see Figures 1 and S1) with previous practical models, and with the almost universally used TLM. The HIV model is included both with the vibrational series fit as proposed in the present work, as well as with two variations to show the insensitivity of the results to the specific fitting procedure.

Model and fitting procedure	G_{inhom}/cm^{-1} ($G_i^{\min.}$/cm^{-1}) [(b)]	$\delta_{abs.}$ [(a)]	δ_β [(c)]	β_0 (10^{-30} esu)
TLM	N.A.	∞	∞	0 - 713[(e)]
Damped TLM				
γ (=1339 cm^{-1}) fitted to absorption	N.A.	8.9 %	13.8 %	649
γ (=1916 cm^{-1}) fitted to β	N.A.	12.0 %	11.3 %	874[3]
HV model (with absorption fit: Eq. (4))	N.A.	0.66 %	4.8 %	514[3]
IV model (with absorption fit: Eq. (4))	N.A.	0.66 %	5.4 %	144[3]
HIV model, with absorption fit:				
vibrational series (Eq. (4)) (k_{vib}=1550 cm^{-1})[(d)]	**1386 (1435)**	**0.66 %**	**2.4 %**	**316**
equidistant series of Gaussians with increasing width (k_{vib}=1550 cm^{-1})[(d)]	1432 (1480)	0.25 %	2.9 %	310
equidistant series of Gaussians with increasing width (k_{vib}=1300 cm^{-1})[(d)]	1370 (1405)	0.14 %	3.5 %	320

[(a)]Root mean square deviation of the absorption fit (% of peak value), taking into account data at second harmonic wavelengths down to 440 nm. [(b)]Smallest Gaussian width among the components of the series. (c) Root mean square deviation (% of peak value) of the fit of the HIV model (taking into account data at second harmonic wavelengths down to 600 nm). [(d)]k_{vib} is the fixed frequency-spacing between the subsequent Gaussian components. [(e)]Depending on experimental datapoint (laser wavelength) used (*e.g.* 29 or 686 × 10^{-30} esu calculated from the β values at 1300 and 1500 nm respectively, or even 871 × 10^{-30} esu from the value measured at 780 nm, close to the high-energy resonance).[3]

Note that in general, when G_{inhom} closely approaches the involved Gaussian widths G_i, one needs to be very cautious in making use of the procedure of Eq. (7). In this case, the substructure of the deconvoluted (*i.e.* homogeneous) absorption spectrum is highly resolved, requiring that the multi-Gaussian fit correctly describes the actual underlying structure of the absorption spectrum.

2. Influence of the incorporation of the higher energy (HE) transition in the HIV β model

2.1 Including the HE transition through a single homogeneously broadened three-level type term

To further test the reliability of the HIV model, the influence of the incorporation of the higher-energy (HE) transition observed in the absorption spectrum of PQDM at 330 nm (see Figure 1) was also explored. Indeed, the underestimation of the values for second harmonic wavelengths below ~625 nm is most likely due to the fact that this additional electronic transition is not considered, and the question rises whether this also affects the static β value. As soon as more than one excited energy level of the molecule is involved, the two-level expression applied *hitherto* (Eq. (2))[1] becomes inadequate, and it is necessary to return to the more general sum-over-states (SOS) expression:[2]

$$\beta_{ijk}(-2\omega;\omega,\omega)=\frac{1}{6\hbar^2}\sum_{m,n}\left(\begin{array}{l}\dfrac{\langle g|\mu_i|m\rangle\langle m|\bar{\mu}_j|n\rangle\langle n|\mu_k|g\rangle}{(\Omega_{mg}-2\omega)(\Omega_{ng}-\omega)}+\dfrac{\langle g|\mu_i|m\rangle\langle m|\bar{\mu}_k|n\rangle\langle n|\mu_j|g\rangle}{(\Omega_{mg}-2\omega)(\Omega_{ng}-\omega)}+\\ +\dfrac{\langle g|\mu_j|m\rangle\langle m|\bar{\mu}_i|n\rangle\langle n|\mu_k|g\rangle}{(\Omega^*_{mg}+\omega)(\Omega_{ng}-\omega)}+\dfrac{\langle g|\mu_k|m\rangle\langle m|\bar{\mu}_i|n\rangle\langle n|\mu_j|g\rangle}{(\Omega^*_{mg}+\omega)(\Omega_{ng}-\omega)}+\\ +\dfrac{\langle g|\mu_k|m\rangle\langle m|\bar{\mu}_j|n\rangle\langle n|\mu_i|g\rangle}{(\Omega^*_{mg}+\omega)(\Omega^*_{ng}+2\omega)}+\dfrac{\langle g|\mu_j|m\rangle\langle m|\bar{\mu}_k|n\rangle\langle n|\mu_i|g\rangle}{(\Omega^*_{mg}+\omega)(\Omega^*_{ng}+2\omega)}\end{array}\right). \quad \text{(S1)}$$

In this expression, ω is the laser frequency and $\Omega_{mg}=\omega_{mg}-i\gamma_{mg}$, with ω_{mg} the excitation frequency of state m and γ_{mg} a homogeneous damping parameter, and $\langle m|\bar{\mu}|n\rangle=\langle m|\mu|n\rangle-\langle g|\mu|g\rangle\delta_{mn}$. The summation runs over all possible combinations of two excited energy levels *n* and *m*, including both non-degenerate three-level type (3LT) terms ($n \neq m$) and degenerate two-level type (2LT) terms for $n = m$ (such as considered in Eq. (2)). Hence, apart from to the 2LT terms involving only the lowest-energy ICT band that were considered in the manuscript (Eq. (2)), the additional terms showing up in the SOS expression[2] are the 3LT terms consecutively reaching the ICT and HE levels, and the 2LT terms with the HE level (see Figure S2).

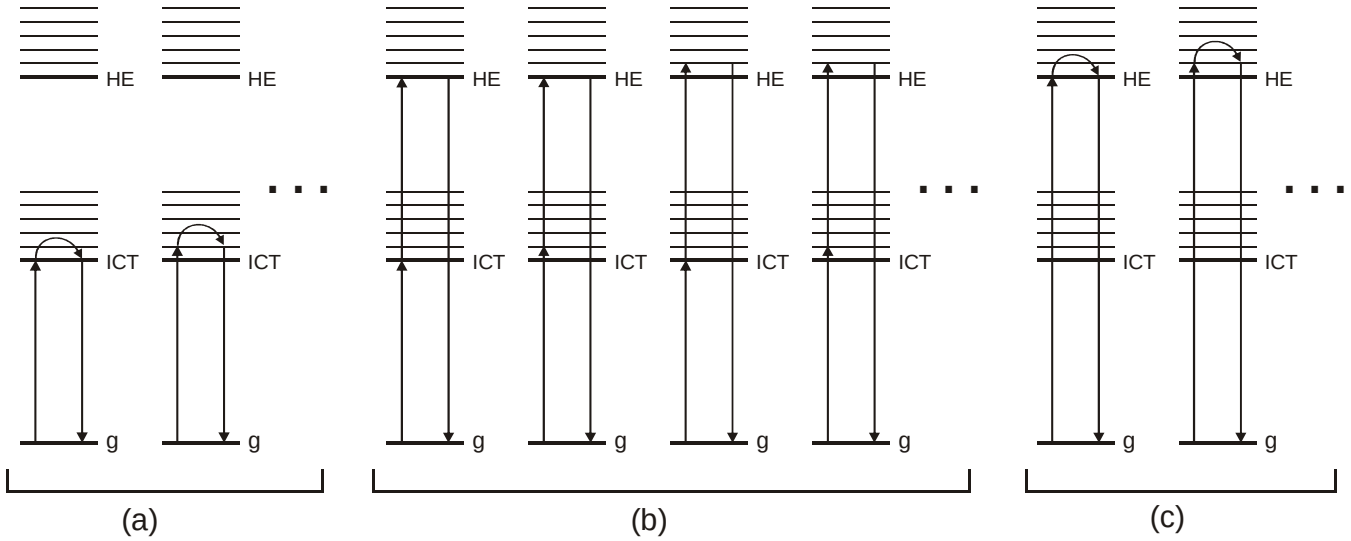

Figure S2. Energy level diagrams representing the different resonance terms in the SOS expression: (a) two-level terms with the lowest-energy ICT level, (b) three-level terms running over the ICT and HE levels and (c) two-level terms with the HE level.

Because including all of these (2LT and 3LT) terms would probably introduce more parameters than necessary, it would be useful to assess which are the most important ones. The relative amplitudes of the terms are determined by (i) the frequency detuning factor (denominators in (S1)) and (ii) the product of the transition dipole moments (μ_i is the i^{th} Cartesian component of the dipole moment operator) between the levels involved (one matrix element for each vertical arrow in Figure S2) and, in case of a 2LT term, by the difference between the dipole moment in the ground state and the excited state (represented by the curved arrow in Figure S2). The impact on β of the 3LT terms (Figure S2(b)) compared to the 2LT terms (Figure S2(c)) is already strongly favored by the frequency detuning factor (especially near double resonance, which is the case here), and is furthermore impacted by the ratio between $\mu_{g\rightarrow ICT} \times \mu_{ICT\rightarrow HE}$ (three-level) and $\mu_{g\rightarrow HE} \times \Delta\mu_{g\rightarrow HE}$ (two-level). As the transition dipole moments starting from the ground state $\mu_{g\rightarrow ICT}$ and $\mu_{g\rightarrow HE}$ are readily available from the linear absorption spectrum (4.5 D and 2.6 D respectively), the unknown factors are the dipole moment difference $\Delta\mu_{g,HE}$ and the transition dipole moment between the two excited states $\mu_{ICT\rightarrow HE}$. Using the λ_{max} values of the ICT and HE bands of PQDM, the 3LT resonance factor (integrated over the resonance

peak around the fundamental wavelength of around 650 nm) is about 30 times larger than the (integrated) 2LT resonance factor, and this ratio remains large (~20-90) for other representative wavelengths within the (inhomogeneous) width of the two bands. Hence, based on these arguments it is to be expected that the 3LT terms will be dominant compared to the 2LT terms, provided that the excited state dipole moment $\mu_{\mathrm{ICT}\rightarrow\mathrm{HE}}$ of PQDM is non-negligible. The latter was checked by means of transient absorption experiments.

Results of these measurements are shown in Figures S3 and S4 (see section 4 below for experimental details). To improve the signal-to-noise (S/N) ratio of the transient spectrum, the data were integrated over the pump-probe delay range of 0.8 to 2.5 ps, excluding the ultrafast response observed at short times (to eliminate any influence of scattered light of the pump beam; anyhow the spectra at short times were very similar), as well as the noisy tails at long times (see Figure S4).

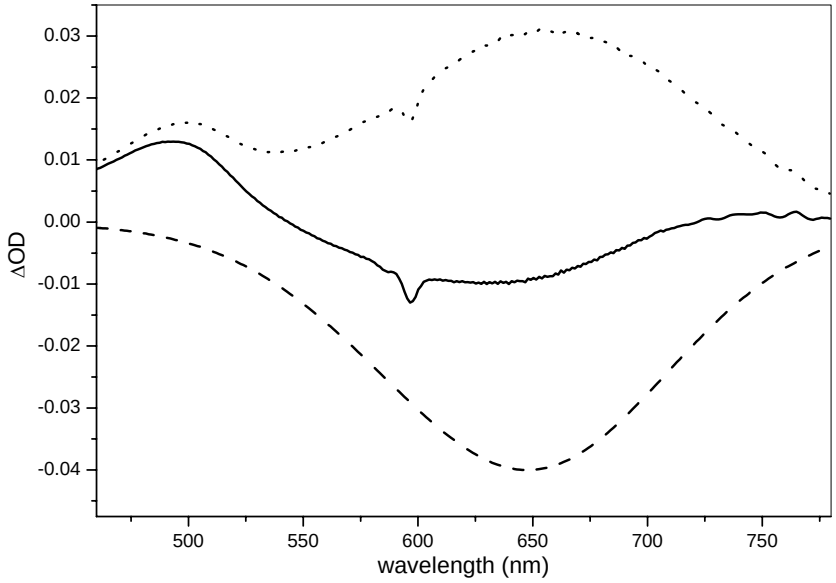

Figure S3. Integrated transient absorption (solid line), and inverted and rescaled linear absorption spectrum (dashed line) of PQDM in *N*,*N*-dimethylformamide (DMF) solution. A narrow feature is observed in the transient spectrum at about 600 nm due to scattering of the pump beam. The dotted line is the transient spectrum corrected for saturable absorption (*i.e.* with the inverted absorption spectrum subtracted), clearly revealing an excited-state absorption band at about 660 nm corresponding to the ICT→HE transition of PQDM, which is used for the determination of $\mu_{\mathrm{ICT}\rightarrow\mathrm{HE}}$.

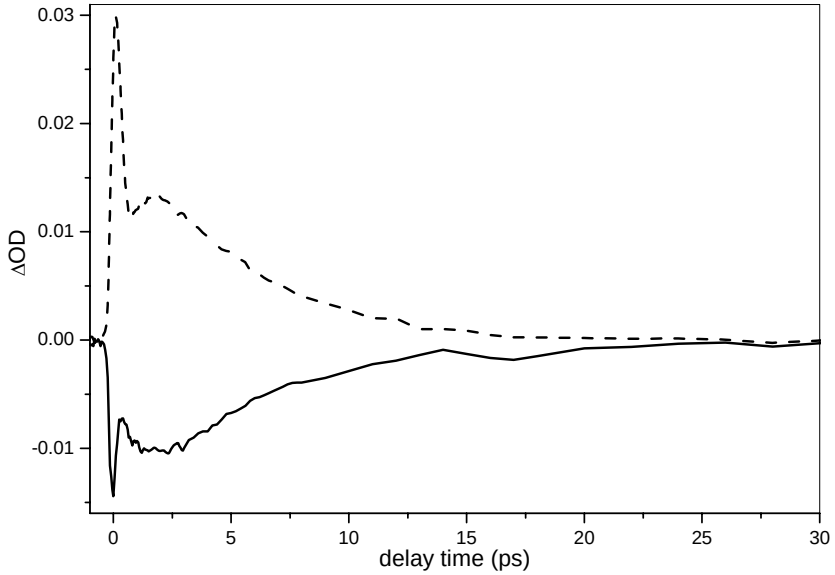

Figure S4. Kinetics of the two bands observed in the transient absorption experiments (Figure S3) at 640 nm (solid line) and at 500 nm (dashed line).

Note that, in addition to the ICT→HE transition at about 660 nm, also an excited-state transition to an even higher-energy state is observed at about 505 nm (see Figure S3), most probably corresponding to the linear absorption band at about 290 nm visible in the linear spectrum (see Figure 1). Unfortunately, the transient absorption from the ICT to the HE state is found to largely overlap with significant saturable absorption (see Figure S3). This is roughly corrected for by subtracting the bleach signal in the form of an inverted and scaled absorption spectrum, which indeed revealed the excited-state absorption band. Assuming that all excited molecules eventually end up in the first excited state and that there is no significant overlapping contribution from stimulated emission (which is only expected at a wavelength longer than 750 nm), the number density of excited molecules was directly determined from the subtracted bleach itself. In spite of these complications, we were able to obtain an (albeit very rough) estimate of $\mu_{\mathrm{ICT}\rightarrow\mathrm{HE}}$ for PQDM of at least around 3 – 4 D (2.6 D as an absolute lower limit based on the fact that subtracting any less leaves negative ΔOD signals), which is clearly a non-negligible value.

Hence, the logical next step in improving the model is the inclusion of the 3LT terms involving the HE transition. However, as these terms involve all combinations of every vibrational level of the ICT state with every vibrational level of the HE state, this is difficult to accomplish and most probably too

detailed in the current case where only the onset of the higher-energy resonance is observed experimentally. Instead, we include only one homogeneously broadened 3LT term, *i.e.* we apply the following expression:

$$(\beta_{incoh}^{SHG}(\omega, G_{in\,\mathrm{hom}}, A, \gamma^{ICT}, \gamma^{HE}))^2 \propto$$

(S2)

$$\int e^{-\frac{\Delta\omega^2}{G_{in\,\mathrm{hom}}^2}} \left\| \int \frac{Abs_{\mathrm{hom}}^{ICT}(\omega'_{eg}+\Delta\omega)}{\omega'^3_{eg}} F(\omega, \omega'_{eg}, \gamma)\, d\omega'_{eg} + A \cdot F_{3L}(\omega, \omega_{eg}^{ICT}+\Delta\omega, \omega_{eg}^{HE}+\Delta\omega, \gamma^{ICT}, \gamma^{HE}) \right\|^2 d\Delta\omega\,,$$

with the three-level term:[2]

$$\begin{aligned} F_{3L}(\omega, \omega_{eg}^{ICT}, \omega_{eg}^{HE}, \gamma^{ICT}, \gamma^{HE}) = {} & \frac{1}{(\omega_{eg}^{ICT} + i\gamma^{ICT} + 2\omega)(\omega_{eg}^{HE} + i\gamma^{HE} + \omega)} + \frac{1}{(\omega_{eg}^{ICT} - i\gamma^{ICT} - 2\omega)(\omega_{eg}^{HE} - i\gamma^{HE} - \omega)} \\ & + \frac{1}{(\omega_{eg}^{ICT} + i\gamma^{ICT} + \omega)(\omega_{eg}^{HE} + i\gamma^{HE} + 2\omega)} + \frac{1}{(\omega_{eg}^{ICT} - i\gamma^{ICT} - \omega)(\omega_{eg}^{HE} - i\gamma^{HE} - 2\omega)} \\ & + \frac{1}{(\omega_{eg}^{ICT} + i\gamma^{ICT} + \omega)(\omega_{eg}^{HE} - i\gamma^{HE} - \omega)} + \frac{1}{(\omega_{eg}^{ICT} - i\gamma^{ICT} - \omega)(\omega_{eg}^{HE} + i\gamma^{HE} + \omega)}\,. \end{aligned}$$

In this expression, A is the relative amplitude of the two-level and three-level contributions, which is determined by the transition dipoles μ and the dipole moment difference $\Delta\mu$ between the involved energy levels, and which is the only additional free parameter compared to the HIV model considering just the lowest-energy transition (Eq. (8)). The homogeneous widths γ^{ICT} and γ^{HE} and the transition frequencies ω_{eg}^{ICT} and ω_{eg}^{HE} are obtained from a fit of the respective absorption band by means of a Voigt profile with the same inhomogeneous width G_{inhom}. Expression (S2) results in a nearly perfect fit to the experimental data over the entire spectral range (see Figure S5) and leads to a static value of 277 × 10^{-30} esu. This value lies within the range set earlier (247 – 397 × 10^{-30} esu)[3] and is not much lower than the β_0 obtained with the HIV model incorporating only the ICT transition (316 × 10^{-30} esu, see above). This confirms the robustness of the HIV model (Eq. (8)) regarding extrapolation of β towards the static limit.

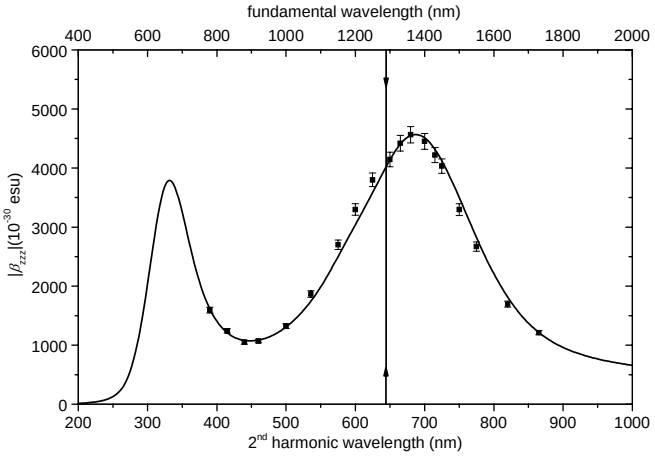

Figure S5. Identical to Figure 2: the HIV model extended with the inclusion of the higher-energy transition by means of a single homogeneously broadened 3LT term (Eq. (S2), curve), fitted to the experimental HRS data of PQDM (squares). The deconvolution width G_{inhom} as well as the overall and relative amplitude are optimized to fit the data, resulting in 1338 cm^{-1} for G_{inhom}, and -4696 for the relative amplitude. Using this G_{inhom}, the homogeneous widths γ^{JCT} and γ^{HE} obtained are respectively 761.1 cm^{-1} and 2220.9 cm^{-1}, and the wavelengths corresponding to the transition frequencies ω_{eg}^{ICT} and ω_{eg}^{HE} obtained are respectively 638.5 nm and 331.8 nm. The vertical arrows indicate λ_{max} of the experimental ICT band (647 nm).

Hence, the incorporation of the higher-energy transition in the β model through a single homogeneously broadened 3LT term is found to yield a correct description of the entire experimental data set, now also including the short-wavelength data points, but this does not affect the extrapolated β_0 much.

2.2 Including the HE transition through two-level type terms

Even though, as explained above, in the present case of PQDM the 3LT terms are expected to yield the dominant contribution from the HE state, an alternative approach might have been to incorporate the HE transition by 2LT terms involving only the ground state and one of the electronically (and vibrationally) excited states (diagrams (c) in Figure S2). Just as a further test of the robustness of the model, we also applied this approach, which can be considered as a worst case, because 2LT terms would be likely to

have a larger effect on β_0, as they fall off more slowly than a doubly-resonant 3LT term. Moreover, this also serves as an example of how in general a 2LT contribution from a HE state can be incorporated.

Here, it is more feasible to include all combinations of vibronic sublevels of both electronic levels, in contrast to the 3LT terms. To do so, the same vibronic fit (Eq. (4)) is applied to the HE absorption band at ~330 nm (see Figure 1) as for the lowest-energy ICT band (*i.e.* ω_{vib} fixed at 1550 cm^{-1} and HWHM fixed at 1196 cm^{-1}). A very reasonable fit with the HE band was obtained with twelve gaussian vibronic bands (the last one being negligible in intensity), with λ_{00} = 396 nm, and S = 3.48 (not shown). For simplicity, the same deconvolution width G_{inhom} is used for both the ICT and the HE transition. This leads to the following expression for the HIV model including a higher-energy transition through 2LT terms:

$$(\beta_{incoh}^{SHG}(\omega, G_{in\,\mathrm{hom}}, A))^2 \propto \int e^{-\frac{\Delta\omega_{HE}^2}{G_{in\,\mathrm{hom}}^2}} \int e^{-\frac{\Delta\omega_{ICT}^2}{G_{in\,\mathrm{hom}}^2}} \left\| \int \frac{Abs_{\mathrm{hom}}^{ICT}(\omega'_{eg} + \Delta\omega_{ICT})}{\omega'^3_{eg}} F(\omega, \omega'_{eg}, \gamma)\, d\omega'_{eg} \right.$$

(S3)

$$\left. + A \cdot \int \frac{Abs_{\mathrm{hom}}^{HE}(\omega'_{eg} + \Delta\omega_{HE})}{\omega'^3_{eg}} F(\omega, \omega'_{eg}, \gamma)\, d\omega'_{eg} \right\|^2 d\Delta\omega_{ICT} d\Delta\omega_{HE}\,.$$

In analogy with Eq. (S2), the parameter A is the relative amplitude of the contributions from both electronic states, which is determined by the $\Delta\mu$ values between the ground level and the two excited levels, and which is the only additional free parameter compared to the HIV model including a single excited energy level. Expression (S3) results in a nearly perfect fit to the experimental data over the entire spectral range (see Figure S6).

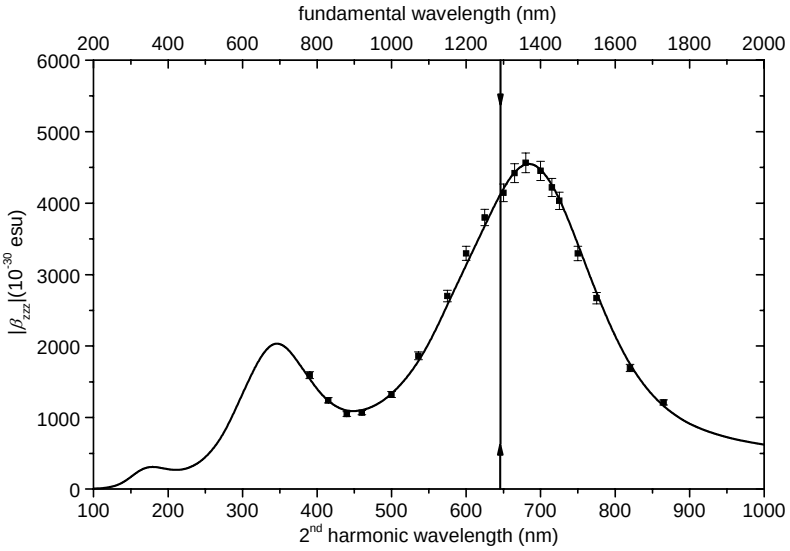

Figure S6. The HIV model including also the higher-energy transition through two-level type terms with uncorrelated inhomogeneous broadening of both transitions (curve), fitted to the experimental HRS data of PQDM (squares). The deconvolution width G_{inhom} (equal for both excited states) as well as the overall and relative amplitude are optimized to fit the data, resulting in 1358 cm^{-1} for G_{inhom}, and -3.5 for the relative amplitude. The vertical arrows indicate $\lambda_{\max}$ of the experimental ICT band.

This leads to a static value of 248×10^{-30} esu, within the range set by the limiting models (albeit very close to the lower limit) and quite similar to the β_0 obtained with the HIV model incorporating only the ICT transition (see manuscript) or also the HE transtion through a single 3LT term (see above).

3. Correlated vs. uncorrelated broadening in the HIV β model including the HE transition

Note that in Eq. S3 the HE transition is inhomogeneously broadened in an uncorrelated way relative to the ICT transition, to avoid the appearance of non-physical sharp peaks in the overlap region of the one-photon resonance with the ICT state and the two-photon resonance with the HE transition. Indeed, in case of correlated inhomogeneous broadening of both transitions, *i.e.* applying the following expression:

$$(\beta_{incoh}^{SHG}(\omega, G_{in\,\text{hom}}, A))^2 \propto \int e^{-\frac{\Delta\omega^2}{G_{in\,\text{hom}}^2}} \left\| \int \frac{Abs_{\text{hom}}^{ICT}(\omega'_{eg} + \Delta\omega)}{\omega'^3_{eg}} F(\omega, \omega'_{eg}, \gamma)\, d\omega'_{eg} \right.$$

(S4)

$$+ A \cdot \int \frac{Abs_{\text{hom}}^{HE}(\omega'_{eg} + \Delta\omega)}{\omega'^{3}_{eg}} F(\omega, \omega'_{eg}, \gamma)\, d\omega'_{eg} \Bigg\|^2 d\Delta\omega ,$$

fine structures are observed in the fundamental wavelength range of 500 – 900 nm (see Figure S7).

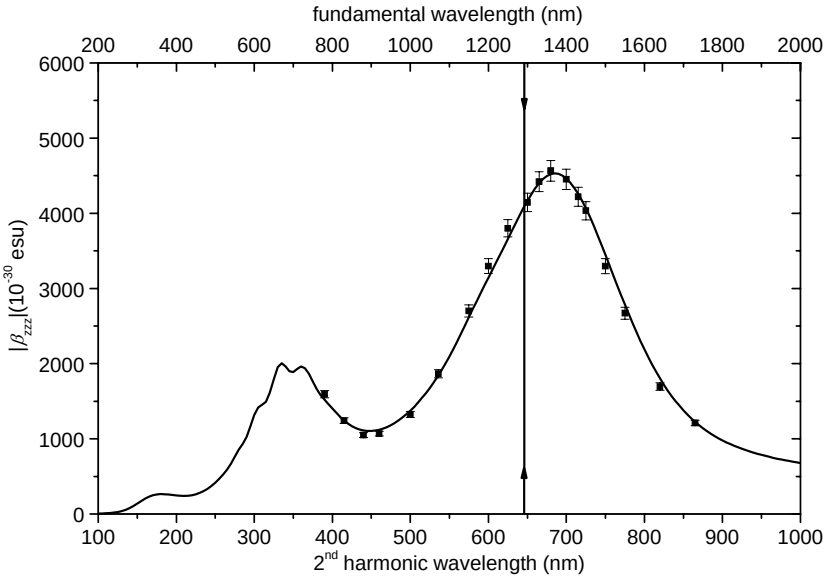

Figure S7. The HIV model including also the higher-energy transition through two-level type terms with correlated inhomogeneous broadening for both transitions (curve) fitted to the experimental HRS data of PQDM (squares). The deconvolution width G_{inhom} of both excited states is set at 1330 cm^{-1}. Subsequently, both the overall and the relative amplitude are optimized to fit the data, which results in -2.9 for the latter. The vertical arrows indicate $\lambda_{\max}$ of the experimental ICT band.

This effect is not expected to be physical, but rather a consequence of the mathematical peculiarities arising in this simplified model. Indeed, the one-photon resonances associated with the ICT band propagate two times faster in the convolution integral than the two-photon resonances originating from the vibrational manifold at higher energy, and both types of resonances are equidistant with the same mutual distance of 1550 cm^{-1}. In this way, some of the one-photon resonances are coinciding with two-photon resonances for several values of the integration variable, and this occurs at some fixed wavelength positions (*i.e.* the positions of the artefacts observed in the final dispersion curve). Despite these artefacts, the choice of correlated/uncorrelated broadening does not influence the static β value very much (281×10^{-30} esu compared to 248×10^{-30} esu as obtained with the uncorrelated approach).

Note that, for the case of the HIV β model including the HE transition through a single 3LT term (Eq. S2), there appears to be no need for (computationally more demanding) uncorrelated inhomogeneous broadening. No sharp structures were observed in this correlated model, and also the overall shape was found to be *quasi*-identical as obtained with the following uncorrelated expression:

$$(\beta_{incoh}^{SHG}(\omega, G_{in\,\mathrm{hom}}, A, \gamma^{ICT}, \gamma^{HE}))^2 \propto \int e^{-\frac{\Delta\omega_{HE}^2}{G_{in\,\mathrm{hom}}^2}} \int e^{-\frac{\Delta\omega_{ICT}^2}{G_{in\,\mathrm{hom}}^2}} \left\| \int \frac{Abs_{\mathrm{hom}}^{ICT}(\omega'_{eg} + \Delta\omega_{ICT})}{\omega'^3_{eg}} F(\omega, \omega'_{eg}, \gamma)\, d\omega'_{eg} \right.$$

(S5)

$$\left. + A \cdot F_{3L}(\omega, \omega_{eg}^{ICT} + \Delta\omega_{ICT}, \omega_{eg}^{HE} + \Delta\omega_{HE}, \gamma^{ICT}, \gamma^{HE}) \right\|^2 d\Delta\omega_{ICT}\, d\Delta\omega_{HE}\,.$$

Using the above expression with the parameters as optimized for the correlated case (G_{inhom} = 1338 cm^{-1}, relative amplitude = -4696) yields a β_0 of 276 × 10^{-30} esu, essentially the same as the correlated value of 277 × 10^{-30} esu.

4. Experimental details of the femtosecond transient absorption setup[4,5]

Briefly, the lasersystem consists of a Ti:Sapphire regenerative amplifier (Spectra-Physics Spitfire), which is seeded by a mode-locked Ti:sapphire laser (Spectra-Physics Tsunami) and pumped by an intracavity doubled diode-pumped Nd:YLF laser (Spectra-Physics Empower). The pulses from the Spitfire (average power ~1 W, repetition rate = 1 kHz, pulse duration ~100 fs, wavelength: 800 nm) are used to pump a computer-controlled ultrafast optical parametric amplifier (OPA; TOPAS-C, Light-Conversion) with unidirectional output (average power ~100 mW), which can be continuously tuned from 1100 to 2800 nm (and second-harmonic: 550 – 1100 nm). In the Helios system, the TOPAS laser beam is used to excite the sample (a liquid solution in a two millimeter path length quartz cell), and a small fraction (approx. 5%) of the Spitfire beam is split off before the TOPAS and used to generate a white-light continuum in a sapphire plate, serving as the probe beam. For the measurements on PQDM, the probe wavelength region was 440 – 850 nm, and the pump wavelength was 600 nm, which is close to the lowest-energy absorption band maximum. The solution was stirred continuously during the data acquisition. The delay between pump and probe is continuously varied within the time range of 0 –

3200 ps by means of a folded delay stage. The repetition rate of the Helios pump beam is reduced from 1 kHz to 500 Hz using a chopper wheel, allowing for a non-pumped (baseline) measurement for every pumped signal spectrum. The measurements were corrected for temporal chirp of the white-light continuum probe.

REFERENCES

(1) Berkovic, G.; Meshulam, G.; Kotler, Z. Measurement and Analysis of Molecular Hyperpolarizability in the Two-Photon Resonance Regime. *J. Chem. Phys.* **2000**, *112*, 3997-4003.

(2) Orr, B. J.; Ward, J. F. Perturbation Theory of the Non-Linear Optical Polarization of an Isolated System. *Mol. Phys.* **1971**, *20*, 513-526.

(3) Campo, J.; Wenseleers, W.; Goovaerts, E.; Szablewski, M.; Cross, G. Accurate Determination and Modeling of the Dispersion of the First Hyperpolarizability of an Efficient Zwitterionic Nonlinear Optical Chromophore by Tunable Wavelength Hyper-Rayleigh Scattering. *J. Phys. Chem. C* **2008**, *112*, 287-296.

(4) Hales, J. M.; Cozzuol, M.; Screen, T. E. O.; Anderson, H. L.; Perry, J. W. Metalloporphyrin Polymer with Temporally Agile, Broadband Nonlinear Absorption for Optical Limiting in the near Infrared. *Optics Express* **2009**, *17*, 18478-18488.

(5) Malicki, M.; Hales, J. M.; Rumi, M.; Barlow, S.; McClary, L.; Marder, S. R.; Perry, J. W. Excited-State Dynamics and Dye-Dye Interactions in Dye-Coated Gold Nanoparticles with Varying Alkyl Spacer Lengths. *Phys. Chem. Chem. Phys.* **2010**, *12*, 6267-6277.